# Practical Observations and Interpretation of Oxide Growth and Exfoliation in Steam

Barry Dooley and Ian Wright

## ABSTRACT

Over the last 40 years oxide growth and exfoliation (OGE) in superheater and reheater tubing have been responsible for a number of power plant problems which seriously have affected reliability. In the same time period, the authors have collected a data base of scale morphologies that has been used to describe in detail the progression of oxide scale development to the point where failure can occur. The concomitant evolution of knowledge of the factors that determine the mode of scale growth and failure in steam has provided the foundation for defining the specific stages in that progression, understanding differences among ferritic and austenitic alloys, and for categorizing the influence of plant operating characteristics. In particular, while tube/steam temperature and the maximum temperature drop at plant shutdown are major variables, the specific cycle chemistry used for the plant feedwater has very little influence. Key stages in the progression of scale growth to the point of failure are identified as OGE indices that are specific for ferritic and austenitic steels. These indices are intended to be used proactively to determine the current condition of a superheater or reheater on the path to exfoliation and possible plant damage. Also, by analyzing samples of exfoliant or oxide deposits responsible for damage, the origin of the oxide, and thus a possible superheater or reheater problem, can be identified retroactively.

## 1 BACKGROUND

Oxide growth and exfoliation of alloys used in superheater and reheater steam circuits have caused numerous problems in the power industry since the late 1960s. Some of these include:

- Short-term overheating (STO) in pendant superheaters (SH) due to accumulation of exfoliated oxide from austenitic alloys at tight (hairpin) bends.
- Solid particle erosion (SPE) of initial blade rows/stages in high-pressure (HP) and intermediate-pressure (IP) steam turbines due to exfoliation from ferritic steels. In extreme cases damage extends through to the initial low-pressure (LP) stages.
- Longterm overheating (LTO) of ferritic alloy tubing due to excessive growth of steam-side oxides due to poor superheater/reheater design, resulting in tubes operating above the Oxidation Limit (OL) for the alloy, or to increasing temperatures as a result of increasing oxide thickness acting as an insulator.
- Deposits throughout steam circuits, sometimes causing sticking of valves.
- Erosion of steam turbine control valves.
- Erosion of bypass valves.
- Deposits in steam turbines causing loss of performance and capacity.
- Exfoliated scale in condensate, contributing to the total iron level.

Concern over the first two issues led in the mid-1970s to efforts to collect and begin to organize data on the various oxide growth and exfoliation (OGE) morphologies and associated service conditions, so that the sources of these damage mechanisms could be identified and understood [1–3]. The present authors have been instrumental in recent years in collaborations to combine the accumulating observations with the development of insight into the mechanisms of oxide growth and exfoliation [4–6]. These efforts led to the concept of an Oxide Growth and Exfoliation Index (OGEI), which is published for the first time in this paper. Understanding of similarities and differences among alloys and alloy classes was recognized to be key to defining the steps leading to scale failure, as well as for projecting the conditions likely to initiate an exfoliation event and the form taken by the material lost. Assembly of these observations into two sets of indices has resulted in a methodology for indicating whether and when such problems can

| Parameter | Range |
|---|---|
| **Ferritic Alloys** | T11, T12, T22, T5, T9, T23, T91 |
| **Austenitic Alloys** | |
| Standard austenitics | TP304H, TP316H, TP321H, TP347H, TP309, TP310HCbN |
| Fine-grained | TPS304H |
| Fine-grained & shot-peened | TP347HFG |
| **Environmental Baselines** | |
| Steam temperature ($T_s$) | saturated and superheated: 1004–1202 °C/540–650 °C |
| Steam pressure ($P_s$) | Sub-critical and super-critical: 290–4873 psi (20–336 bar) |
| Tube temperature ($T_m$) | Range up to 1202 °F/650 °C |
| Feedwater cycle chemistry | AVT and OT with oxygen levels ranging from 1–400+ $\mu g \cdot L^{-1}$ |

Table 1:
Materials and environments of superheater/reheater steam circuits.

| | |
|---|---|
| AVT(R) | all-volatile treatment under reducing conditions |
| AVT(O) | all-volatile treatment under oxidizing conditions |
| OT | oxygenated treatment |

be expected by examining superheater/reheater tube samples removed for metallurgical analysis. In addition, this approach allows identification of the exact source of the exfoliated oxide that has caused the damage delineated above.

To help in understanding the practical importance of OGE, the following introductory sections are included to summarize the main features which relate directly to the suggested OGEI. The materials and the steam environments of focus for this paper are included in Table 1. The compositional specifications for the alloys are summarized in Table 2.

## 1.1 General Introduction to Oxide Growth

Generally, scales growing in steam on the alloys listed in Table 2 exhibit morphologies that consist typically (at least initially) of two main layers. The layer next to the alloy usually is referred to as an "Fe-Cr spinel" (abbreviated in this paper as 'L1'), and the main outer layer is "magnetite" ($Fe_3O_4$, abbreviated in this paper as 'L2'), see Figure 1. In simple parlance, the interface between L1 and L2 represents the original alloy surface, with L1 taken to grow inwards, and L2 outwards. In fact, both layers are basically magnetite (which has a spinel structure), but while L1 contains elements incorporated from the alloy as the oxide front progresses inward (chiefly Cr, but also Mn, Si, Mo, etc.), L2 is essentially pure magnetite by virtue of its growing by outward diffusion of iron ions.

With continued scale development, changes occur in the morphologies of both original layers that require more detailed descriptions than suggested by 'L1' and 'L2.' This is especially the case for the original L1 on ferritic steels, where new layers may form in addition to (or from) growth of the original L1. These changes result largely from the participation of chromium in the scale-forming process and its effect on slowing scale growth, and can be used to discriminate in particular among the behaviors of alloys T22, T23, and T91. The changes that occur in the original L2 are similar for the ferritic and austenitic steels: while the thickness of the original L2 increases with time, under some circumstances the magnetite is further oxidized to hematite ($Fe_2O_3$). The hematite forms along the original L2-steam interface at the expense of the magnetite, and may eventually occupy a large fraction of the space that otherwise would be described as 'L2.'

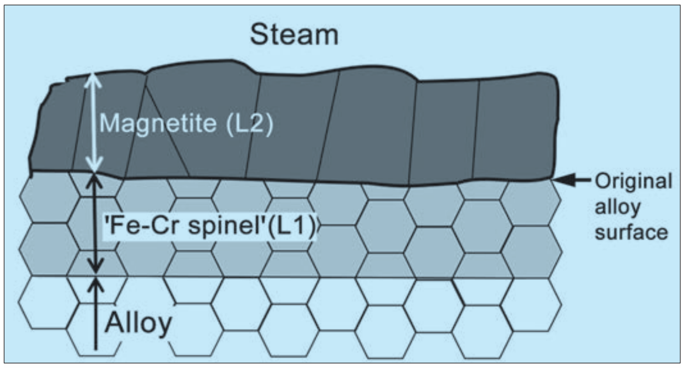

Figure 1:
Schematic diagram of a cross section of the initial scale typically formed in steam on ferritic steels containing up to 9 wt% Cr.

| Alloy | Composition [wt%] | | | | | | | | | | | | |
|---|---|---|---|---|---|---|---|---|---|---|---|---|---|
| | **Cr** | **Ni** | **Si** | **Mn** | **C** | **S** | **P** | **Mo** | **V** | **Nb** | **Ti** | **W** | **Cu** |
| T12 | 0.8–1.25 | | 0.5 | 0.3–0.61 | 0.05–0.15 | 0.025 | 0.025 | 0.44–0.65 | | | | | |
| T11 | 1.0–1.5 | | 0.5–1.0 | 0.3–0.6 | 0.05–0.15 | 0.025 | 0.025 | 0.44–0.65 | | | | | |
| T22 | 1.9–2.6 | | 0.5 | 0.3–0.6 | 0.05–0.15 | 0.025 | 0.025 | 0.87–1.13 | | | | | |
| T23 | 1.9–2.6 | | 0.5 | 0.1–0.6 | 0.04–0.1 | 0.01 | 0.03 | 0.05–0.3 | 0.2–0.3 | 0.02–0.08 | | 1.45–1.75 | |
| T5 | 4–6 | | 0.5 | 0.3–0.6 | 0.15 | 0.025 | 0.025 | 0.45–0.65 | | | | | |
| T9 | 8–10 | | 0.25–1.0 | 0.3–0.6 | 0.15 | 0.025 | 0.025 | 0.9–1.1 | | | | | |
| T91 | 7.9–9.6 | | 0.18–0.56 | 0.25–0.66 | 0.06–0.15 | 0.012 | 0.025 | 0.8–1.1 | 0.16–0.27 | 0.05–0.11 | | | |
| TP304H | 18–20 | 8–10.5 | 0.75 | 2 | 0.04–0.1 | 0.03 | 0.045 | | | | | | |
| TP316H | 16–18 | 10–14 | 0.75 | 2 | 0.04–0.1 | 0.03 | 0.045 | 2–3 | | | | | |
| TP321H | 17–19 | 9–12 | 0.75 | 2 | 0.04-0.14 | 0.03 | 0.045 | | | | a | | |
| TP347H | 17–19 | 9–13 | 0.75 | 2 | 0.04–0.1 | 0.03 | 0.045 | | | b | | | |
| TP347HFG | 17–20 | 9–13 | 0.75 | 2 | 0.06–0.1 | 0.03 | 0.04 | | | b | | | |
| Super304H | 17–19 | 7.5–10.5 | 0.3 | 1 | 0.07–0.13 | 0.001 | 0.004 | | | 0.3–0.6 | | | 2.5–3.5 |
| TP309 | 22–24 | 12–15 | 1 | 2 | 0.2 | 0.03 | 0.045 | | | | | | |
| TP310HCbN/HR3C | 24–26 | 19–22 | 1 | 2 | 0.04–0.1 | 0.03 | 0.045 | | | 0.2–0.6 | | | |

Table 2
Compositional specifications of alloys. The preferred ranges for key elements are shown, while a single value denotes the maximum allowable.
a: 4 x (C + N) to 0.7 max
b: 8 x (C + N) to 1 max

| | | | | | | | | | | | | | |
|---|---|---|---|---|---|---|---|---|---|---|---|---|---|
| **Cr** | chromium | **Si** | silicon | **C** | carbon | **P** | phosphorus | **V** | vanadium | **Ti** | titanium | **Cu** | copper |
| **Ni** | nickel | **Mn** | manganese | **S** | sulfur | **Mo** | molybdenum | **Nb** | niobium | **W** | tungsten | **N** | nitrogen |

Because at the temperature of operation (Table 1) these oxides are semiconductors, they grow by diffusion of iron ions (mostly $Fe^{2+}$) outwards and oxidant inwards (the oxidant typically is considered to consist of oxide ions ($O^{2-}$)) [4]. Hence, growth of the magnetite layer (L2) occurs at the oxide-steam interface, and Fe-Cr spinel (L1) at the oxide-metal interface. Scale thickening as a result of these counter diffusion processes initially follows a parabolic rate law.

It is also important to note that the oxide growth processes are not dependent on the cycle chemistry used in the feedwater circuits of the plants (AVT(R), AVT(O) or OT) [7], nor specifically on the dissolved oxygen level. Oxide growth is dependent on the partial pressure, *p*, of oxygen from the equilibrium dissociation of steam, via:

$$H_2O(g) \Leftrightarrow H_2(g) + 1/2O_2(g) \tag{1}$$

for which:

$$k_1 = (pO_2)_{eq}^{0.5} \times pH_2/pH_2O \tag{2}$$

and $k_1$ is calculated from the known free energy of the dissociation reaction. As shown in Figure 2 values of $pO_2$ from the dissociation of steam are several orders of magnitude higher than those for the formation of the various oxides considered. "Reducing" conditions associated with AVT(R) feedwater treatments (usually $< 10\,\mu g \cdot kg^{-1}$ oxygen plus a reducing agent) re-

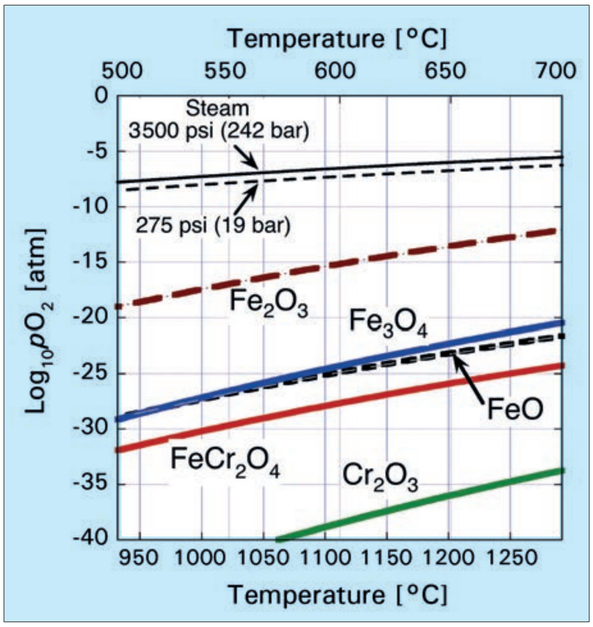

Figure 2:
Comparison of the oxygen partial pressures ($pO_2$) for the formation of the oxides of interest; those resulting from the equilibrium dissociation of steam also are included [4].

sult in an effective $pO_2$ of the order of $10^{-9}$ atm ($\log_{10}pO_2$ value of –9.0), which also is several orders of magnitude higher than for the oxides. For OT conditions involving oxygen additions of 20 or $200\,\mu g \cdot kg^{-1}$, the effective $pO_2$ ranges from $2.2 \times 10^{-6}$ to $2.9 \times 10^{-5}$ atm ($\log_{10}pO_2$ values of –5.6 to –4.5), higher than for the dissociation of steam. Overall, from thermodynamic considerations, all the oxides (including hematite) are expected to be stable under all boiler steam conditions, though wüstite (FeO) often may be absent due to kinetic considerations.

Often, hematite is observed to be absent from such scales, and this also is a result of overriding kinetic factors. Since magnetite is thermodynamically more stable than hematite (i.e., can form at lower oxygen partial pressures), and since hematite grows by further oxidation of magnetite, in situations where the availability of iron ions at the scale-steam interface is greater than that of oxidant, magnetite will form in preference to hematite. This typically is the situation during the early stages of scale growth and/or when outward transport of iron ions outward from the alloy is less impeded by blocking. When such blocking does occur, a point will be reached where the relative availability of iron ions at the magnetite-steam interface diminishes, and the existing magnetite will start to be oxidized to hematite. This is an important point because very often the appearance of hematite along this interface has been interpreted mistakenly as being related to the oxygen level in the steam. The general further development of the duplex layers and hematite are covered later in the OGEI sections (Section 2).

### 1.2 General Introduction to Exfoliation

The initial duplex oxide scales grow in an essentially stress-free state at high temperatures because of the equal counter flux diffusion processes indicated previously. Any stresses experienced are accommodated by adjustment of the morphology of the growing scale and possibly by creep. For the ferritic alloys that subsequently develop multi-laminated scales, growth stresses are generated in the overall oxide layers because of the confined space. Additional stresses can arise during scale growth from physical considerations such as constraint from the curved tube surfaces, and from operational factors such as periodic variations in steam temperature and pressure. However, the largest and most consequential stresses are from the differential contraction that occurs between the alloy and scale (and among scale components) during cooling upon unit shutdown.

Table 3 lists values of the coefficients of thermal expansion (CTE) for ferritic and austenitic steels and oxides of interest, and illustrates the higher values for austenitic steels and the large differences between the steels and magnetite and hematite. No separate value for the CTE of Fe-Cr spinel (i.e., L1) is shown, since practical measurements have indicated that it closely tracked the upper bound of the values for "pure" magnetite (as listed in the "revised" values in Table 3). This finding was true for the range of chromium levels found in Fe-Cr spinels formed on T91 and standard austenitic steels [8].

Examples of calculated oxide-metal strains after cooling from 1112 °F/600 °C to ambient are shown in Table 4. The cooling strains are directly related to the magnitude of the temperature drop, not to the rate of temperature change. This is an important practical point as it implies that exfoliation on austenitic materials does not occur until a boiler has cooled almost to ambient, and that shorter shutdowns ("hot," "warm") may not be accompanied by exfoliation. From these CTE data it is evident that the cooling strains on ferritic steels are tensile, and are smaller than the compressive strains experienced on austenitic steels. Also shown is the large influence of the presence of hematite (assumed in calculations to be a uniform layer along the outer magnetite (L2)-steam interface); a value for 20 % hematite (by thickness) is shown as an example, but this

| | CTE ($K^{-1}$ x $10^{-6}$) [1] | | CTE ($K^{-1}$ x $10^{-6}$) Revised 2019 [9] | |
|---|---|---|---|---|
| | 572 °F/300 °C | 1112 °F/600 °C | 572 °F/300 °C | 1112 °F/600 °C |
| T22 ferritic | 14.0 | 16.2 | 12.9 | 13.7 |
| T91 ferritic | — | — | 12.2 | 12.4 |
| TP300-series austenitics | 18.6[a] | 19.5[a] | 17.5[b] | 18.7[b] |
| Magnetite | 14.25 | 16.5 | 10.4±1.3 | 13.4±1.4 |
| Hematite | 11.9 | 12.9 | 10.0 | 11.8 |

Table 3:
Examples of differences in coefficients of thermal expansion for alloys and oxides.
a: TP316
b: TP347

| | T22 Ferritic | TP316 Austenitic |
|---|---|---|
| Scale with 0 % $Fe_2O_3$ | 1 x $10^{-4}$ tension | 1.8 x $10^{-3}$ compression |
| Scale with 20 % $Fe_2O_3$ | 0.5 x $10^{-4}$ tension | 2.0 x $10^{-3}$ compression |

Table 4:
Examples of oxide-metal strains on cooling from 1112 °F/600 °C to ambient for tube materials with scales having different levels of hematite along the oxide-steam interface [10].

effect continues to increase with increasing levels of hematite.

Calculations of the critical strains at which individual oxides will fail as a function of scale thickness and mode of failure have been used to create "oxide failure maps" such as that shown in Figure 3 [after reference 1]. Note that in this map, negative values of strain are tensile in the oxide, and positive values are compressive in the oxide. Such maps allow visualization of the critical strain or oxide thicknesses ($d_{crit}$) at which failure will occur according to the specific mode expected for given alloy/scale combinations. For scale failure in tension, there exist models describing several different modes, including by through-scale cracking, and by the formation of multi-laminations [11], clearly indicating the influence of scale morphology.

Superimposed on the map in Figure 3 are results from measurements on scales formed on ferritic and austenitic steel superheater tubes. These clearly indicate that scales on ferritic steels fail (in tension) at greater thicknesses than on austenitic steels (in compression). The vertical lengths of the superimposed data points in Figure 3 further illustrate the influence of the presence of hematite in such scales. As expected from the results in Table 4, the presence of hematite in the scale on a ferritic steel decreases the tensile stress/strain and effectively delays exfoliation to greater scale thicknesses, whereas for an austenitic steel hematite causes earlier exfoliation.

While maps such as Figure 3 can indicate when scale failure is expected, and generally by which mode, an important practical consideration is to be able to define the conditions under which actual loss of scale will occur, and the characteristics of the material exfoliated. For scales formed on ferritic alloys that are subjected to tensile stresses on cool down the map indicates that the likely first step in exfoliation is through-scale cracking. Actual loss of scale requires the further step of decohesion, which would occur preferentially along planes of weakness in the scale, such as voids along interfaces.

For scales formed on austenitic alloys that are subjected to compressive stresses on cool down the tendency will be for the scale to buckle. Scenarios for expected modes of exfoliation range from local decohesion along a plane of weakness and lifting of the affected scale, followed by through-cracking of the scale at the ends of the buckle and detachment of the lifted scale, to (absent an obvious plane of weakness) initiation by the formation of inclined shear cracks in the scale, followed by local decohesion between these cracks, lifting, and loss of the affected flake of scale [11]. In the exfoliation routes where decohesion is the final step, separation of oxide segments may not occur immediately following the cracking event; additional stresses from continued oxidation due to ingress of steam along the cracks may be needed [12]. Overall, in any of these scenarios it is obvious that the detailed morphology of the scale plays an important role in determining the route taken by the exfoliation process, and the form of the material that detaches.

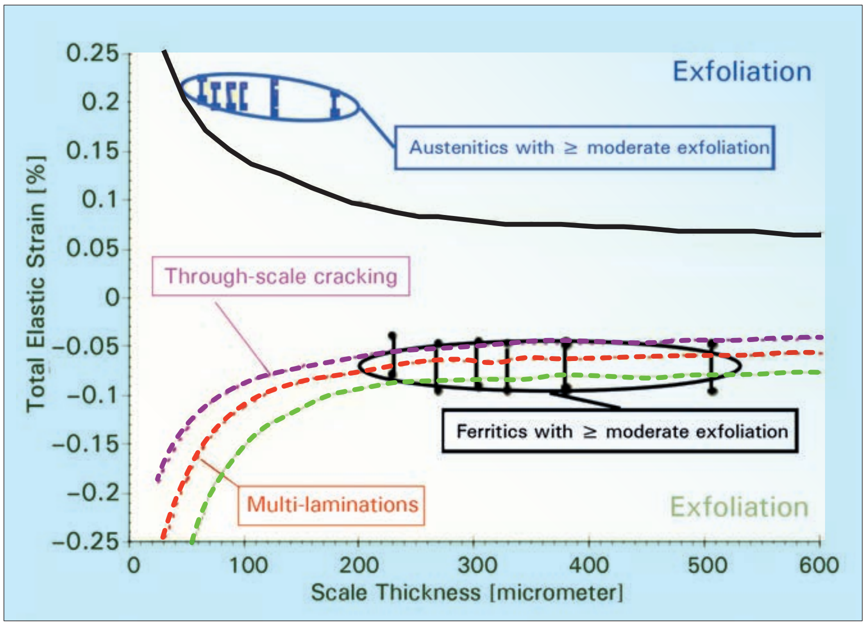

Figure 3:
Map of failure modes of oxides as a function of imposed strains [after reference 1], with superimposed results from measurements of scales formed on austenitic and ferritic steel superheater tubes [10].

## 2 INTRODUCTION TO THE OXIDE GROWTH AND EXFOLIATION DATA BASE

This section of the paper comprises two main parts. The first describes the morphological developments with increasing time for the scales formed on ferritic steels, and shows the progression of OGE as described by OGEI Numbers 1 to 5. The second part shows the progression of OGE for austenitic steels by OGEI Letters A to E. The description of each index includes the morphological features of each stage. For some alloys in a given class there can be major differences in the morphologies of the scales formed in steam, for example, between ferritic steels T22 and T23 or T91, and between austenitic alloys with and without shot peening. Such differences are highlighted because of the importance of being able to recognize the source of exfoliant found to be associated with damage or failure. Recent comprehensive compilations of representative scale morphologies are available [5,13].

### 2.1 Oxide Growth and Exfoliation Indices for Ferritic Steels – Alloys Considered: T11, T12, T22, T23, T91

**OGEI 1: In this stage the initial, characteristic duplex scale structure is formed.**

On all the ferritic steels of interest for service in steam (typically with chromium contents below about 11 wt%) an initial duplex oxide is formed that consists of an inner layer of Fe-Cr spinel (L1) and an outer layer of magnetite (L2), as suggested in Figure 1. This morphology is seen most often on alloys T11, T12, and T22 operating at the lower temperatures of superheaters and reheaters, and an example is shown in Figure 4. There is no evidence of any laminations or formation of alternate layers beneath this initial duplex pair, and no hematite decoration on the outside of the magnetite layer (L2), even after very long times of operation. At "low temperatures" this morphology remains for long times, and may never change into an OGEI 2 morphology. At higher temperatures this initial morphology breaks down into the OGEI 2 and 3 morphologies at relatively early operating times.

**OGEI 2: This index stage involves the first breakdown of the initial duplex pair.**

Initial breakdown involves the formation of a second duplex pair of oxides at the original Fe-Cr spinel/tube interface (i.e., the alloy-L1 interface), followed by the initiation of further duplex pairs at the same interface. Figure 5 shows an example: the original duplex pair still is identifi-

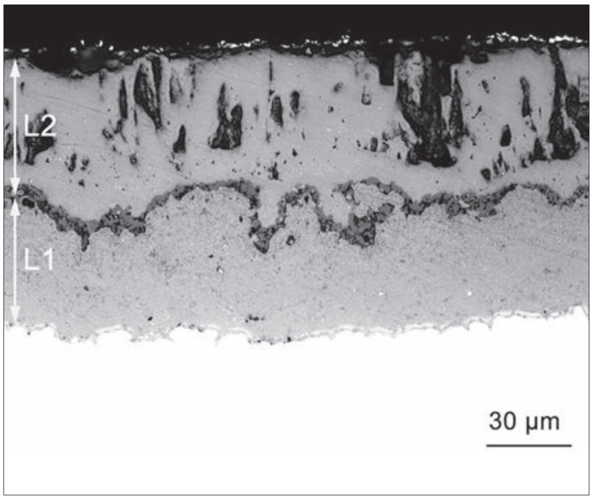

Figure 4:
Initial duplex oxide on alloy T22 after 158 000 h at a steam temperature of 900 °F/480 °C.

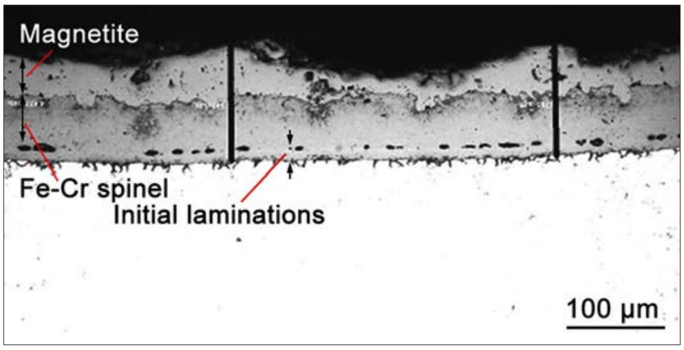

Figure 5:
Example of OGEI 2 on alloy T22 showing initial formation of laminations at the base of the original Fe-Cr spinel (L1) of the initial duplex pair after 149 000 h (3 120 starts) at an estimated temperature of 980 °F/526 °C (note: the two black lines were inscribed to measure oxide thickness).

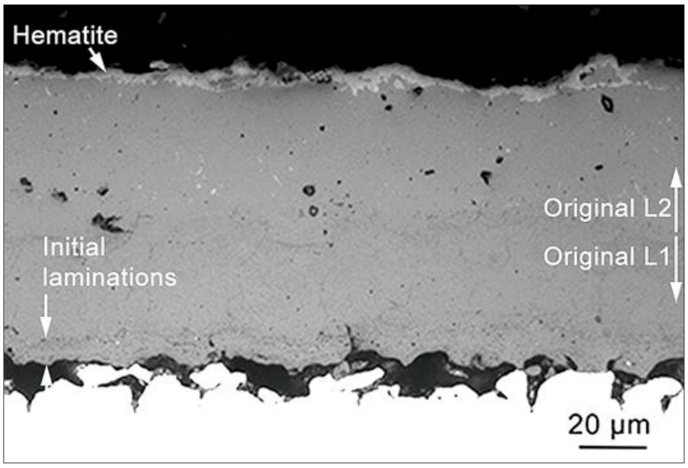

Figure 6:
Further example of OGEI 2 on alloy T22 showing initial formation of laminations at the base of the original Fe-Cr spinel (L1) of the initial duplex pair, and formation of hematite on the outer surface of the original magnetite layer (L2).

able at this stage, even though a number of laminations (repetitive duplex pairs) are present. In addition, voids can be seen along the interfaces between duplex pairs. In some cases, especially where these voids are more continuous, there will be indications of hematite along the outer magnetite surface (Figure 6 shows an example).

These repeating pairs of Fe-Cr spinel and magnetite layers at the alloy-original L1 interface are much thinner than the original duplex pair (L1/L2), and are always oriented with the Fe-Cr spinel nearest the alloy surface. Also, the Fe-Cr spinel in these pairs has a very small grain size, while in the corresponding magnetite layer the grains are significantly larger, apparently columnar, and include intermixed porosity [6].

### OGEI 3: In this stage there starts to be a difference in the morphologies of scales formed on alloys T11/T12/T22, T23, and T91.

For alloys T11/T21/T22, OGEI 3 is characterized by an increasing number of distinct laminations consisting of repetitive duplex pairs which gradually consume the original Fe-Cr spinel (L1). Lines of voids are evident within the laminated structure. Examples of these features in scales on alloys T12 and T22 are shown in Figure 7.

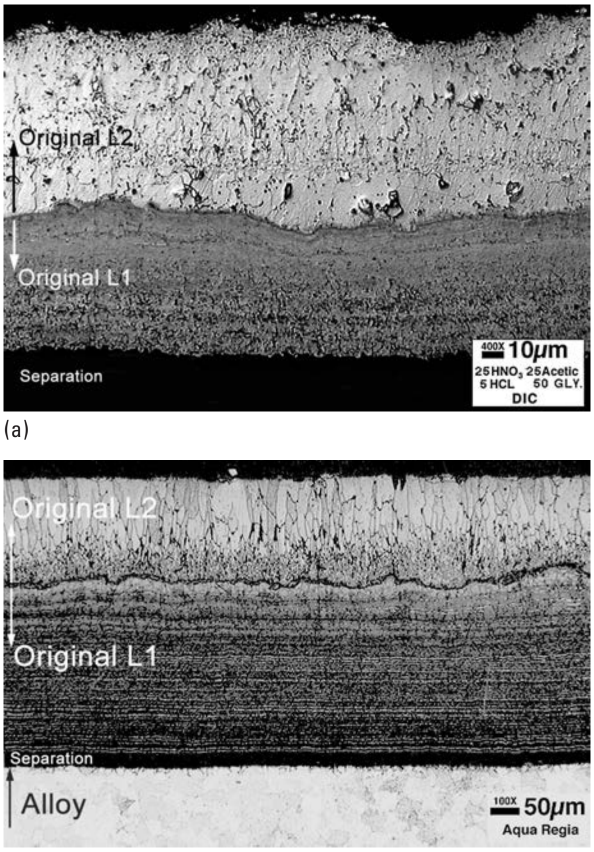

(a)

(b)

Figure 7:
Example of OGEI 3 for (a) 155 µm-thick scale on alloy T12, and (b) 475 µm-thick scale on alloy T22 from secondary and tertiary reheater outlets, respectively, of the same boiler ($T_s$ = 1 056 °F/569 °C).

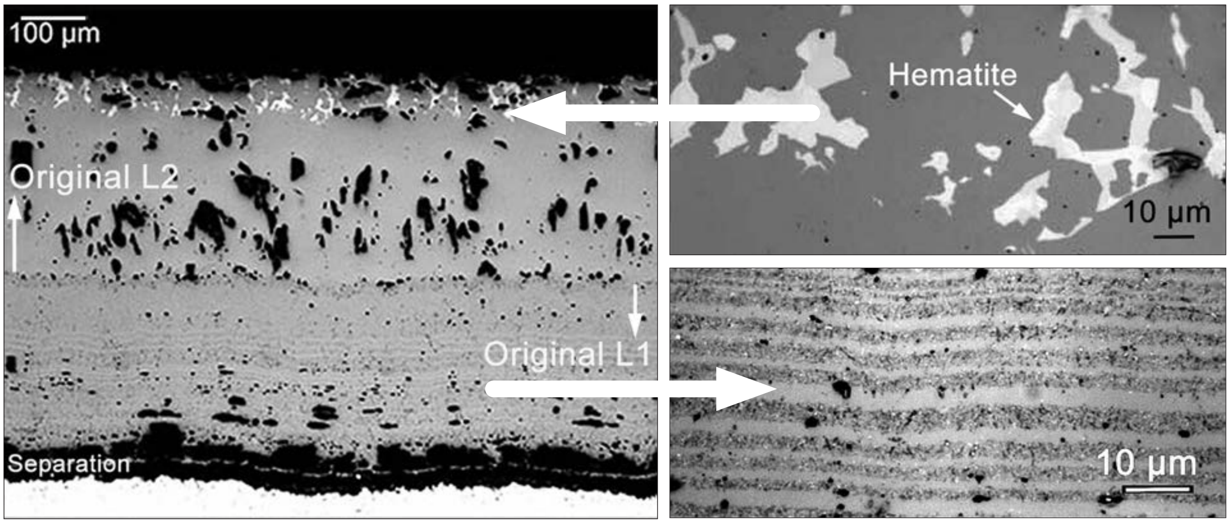

Figure 8:
Example of OGEI 3 for alloy T23 after 31 000 h at 1 050 °F/565 °C, showing (right bottom): the varying thickness of the alternate layers, and (right top): hematite formation at the original L2-steam interface.

For alloy T23, OGEI 3 is characterized by an increasing number of alternate layers of Fe-Cr spinel and magnetite (duplex pairs) which always vary considerably in thickness, Figure 8, unlike the laminations in the scales on T11 and T22, which typically are of similar thickness. Further, unlike for T22, on T23 these alternate layers initiate immediately below the original magnetite layer (at the original L1-L2 interface). In addition, there is usually some obvious hematite along the outer magnetite-steam interface (as indicted in Figure 8).

As with alloy T22, the alternate layers of magnetite and Fe-Cr spinel on T23 are readily identified from X-ray maps for iron and chromium, as shown in Figure 9.

For T91, the detailed morphology of the overall inner layer differs from that on the lower-Cr alloys in that instead of alternating Cr-rich/Fe-rich laminations, the distribution of chromium in this layer takes the form of Cr-rich bands. In fact, the overall inner layer on T91 has no features to suggest alternating layers with different structures or morphologies like T22 [6] as illustrated in Figure 7b. The bands have a higher chromium level than the laminations, and consist of discrete grains or subgrains of Fe-Cr spinel ($FeCr_2O_4$) surrounded by magnetite ($Fe_3O_4$).

This change in the morphology of the overall inner layer compared to the lower-Cr ferritics is directly related to the distribution of chromium in the ferritic-martesitic lattice of the 9-Cr alloys [5]. The specific morpho-logy of the martensitic laths in the alloy depends on its composition and heat treatment, which in turn influence the structure and chromium content of the Cr-rich bands in the scale.

During initial oxide growth, chromium enters the inner layer (L1) with a similar distribution to that in the alloy, as the chromium carbide lattice of the alloy is oxidized in-situ. Further, these bands appear to be present in the overall inner layer almost from the beginning of scale formation. Hence, blocking of outward iron ion trans-

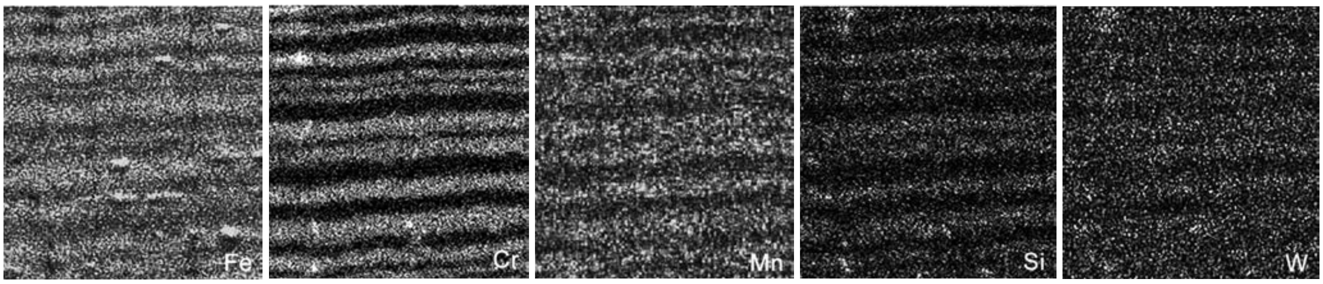

Figure 9:
Elemental X-ray maps for the alternate duplex layers formed in the original inner layer on alloy T23, indicating that these pairs consist of alternate magnetite (Fe-rich) and Fe-Cr spinel (Cr-rich) layers, and showing the co-location of Mn, Si, and W with the Cr.

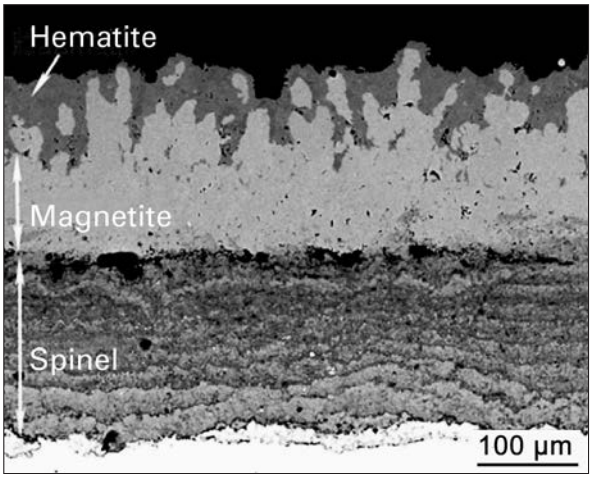

Figure 10:
Example of OGEI 3 for T91 after 63600 h at 1051 °F/566 °C, showing a distinct banded structure in the overall inner layer, voids at the base of the original magnetite, and hematite in the original magnetite (in this scanning electron microscope back-scattered image, hematite appears darker than magnetite).

port will occur from the start and increase as the number of bands increases with time. Typically, hematite is considered to form earlier on T91 compared with alloys T11/12/22 and T23.

The OGEI 3 stage for alloy T91 usually is associated with the formation of a semi-continuous layer of voids along the base of the original magnetite (original L1-L2 interface), and hematite decoration on the outer surface of the original magnetite (original L2-steam interface). These features result initially from increased restriction of the outward diffusion of iron ions by the blocking action of the chromium-rich bands.

Figure 10 shows an example of the typical appearance in scale formed on T91 in steam of these Cr-rich bands in the overall inner layer, voids along the base of the original magnetite, and hematite along the outer surface of the original magnetite, all of which are a direct consequence of reduced transport of iron ions across the overall inner layer. The corresponding elemental X-ray maps shown in Figure 11 clearly identify the high chromium levels in the bands in the overall inner layer, and suggest that while Si also is present, it only co-locates with chromium in the bands later in the oxidation process (nearer the alloy surface). The presence of silicon with chromium in the bands would significantly increase their blocking power. Additionally, in some situations the voidage in the scales on T91 spreads along the base of the original magnetite, and may increase sufficiently that delamination of the original magnetite (and associated hematite) eventually occurs.

Overall, OGEI 3 for this range of ferritic steels is a key stage that allows unique distinctions to be made by analysis of oxide flakes collected in an area of plant failure or damage. Some of the laminated or banded structure "consumes" the Fe-Cr spinel/L1 of the original duplex pair until it disappears or is not visibly distinct. For alloys T11, T12, and T22 this inner structure becomes multi-laminated. For T23 there are very distinct wider layers of unequal thickness. On T91 this inner structure takes the form of non-continuous bands of more highly chromium-rich regions within the overall inner layer. In all cases, voids that start to appear at the base of the original magnetite are associated with the laminations, layers, and bands. Formation of hematite at the outer surface of the original magnetite usually appears coincidentally with these developments.

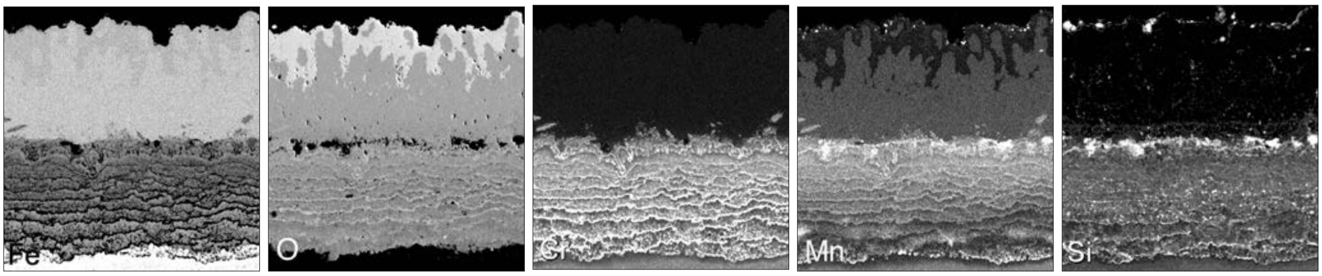

Figure 11:
Elemental X-ray maps for the scale shown in Figure 10, indicating the Cr-rich bands in the overall inner layer, as well as the co-location with the Cr of Mn in the top portion, and of Si in the bottom portion of this layer.

### OGEI 4: This stage involves initiation of exfoliation (essentially, the origination of cracks).

For alloys T11, T21, and T22, as the thickness of the multi-laminated structure increases, cracks start to appear perpendicular to the alloy/scale interface. Most often such cracks do not propagate through the full thickness of the multilayers, and may be contained "within" the scale, as suggested in Figure 12 for alloy T22; the original Fe-Cr spinel is indicated in location No. 3, while the multi-laminated structure consisting of multiple duplex pairs is found in location No. 2. In such cases, no scale exfoliation may have occurred.

Cracks similar to those seen in T22 develop perpendicular to the alloy-oxide interface in scales on T91, but may not be obviously damaging to the integrity of the scale; some apparently "heal" (Figure 13).

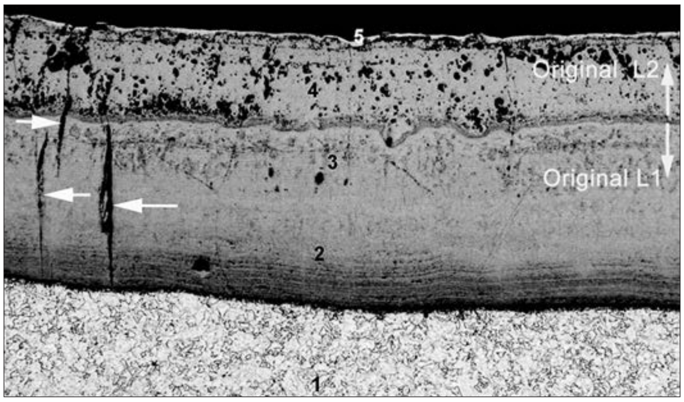

Figure 12:
Example of OGEI 4 for alloy T22 showing initiation of exfoliation as cracking perpendicular to the alloy-scale interface (arrows).

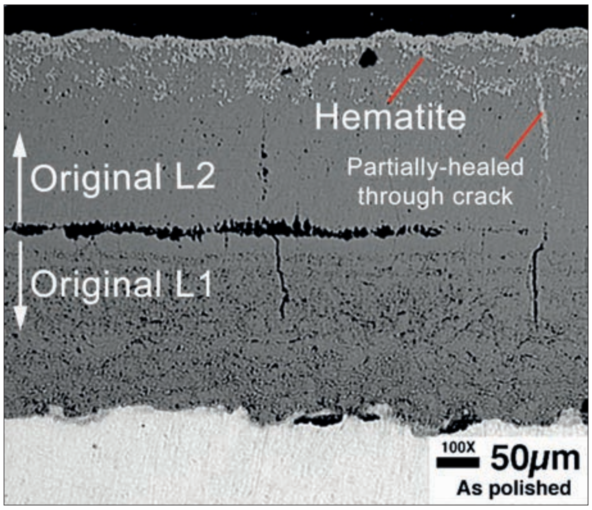

Figure 13:
Example of OGEI 4 for a 475 μm-thick scale on T91 showing propagation of cracks perpendicular to the alloy surface in the overall inner layer and the original magnetite, voidage along the original duplex interface, a banded structure in the original L1, and hematite on the outer magnetite surface (after 15 500 h at 1 026 °F/552 °C).

### OGEI 5: This is the stage where actual scale loss by exfoliation occurs.

For T11, T12, T22, and T91 the mode of exfoliation involves variants of crack formation perpendicular to the alloy-oxide interface, followed by separation along planes of weakness in the scale. Such planes usually involve voids associated with the multi-laminations (T11, T12, T22), or voids accumulated along the base of the original magnetite (T91). Sometimes exfoliation takes place perpendicular to the alloy-oxide interface. Exfoliant from T23 is similar to T11/T12/T22, but the alternate layers of spinel and magnetite in the inner layer involved are much more distinct (wider, and of unequal thickness).

Exfoliation from T11/12 and T22 can produce flakes having a range of sizes, and loss may occur multiple times from the same location, especially on T22, Figure 14. Such exfoliant typically comprises thick flakes of oxide containing the magnetite (L2) from the original duplex pair and part of the original Fe-Cr spinel layer (L1) containing (usually several) multi-laminations, as indicated in Figure 15. These flakes of oxide can become entrained in the steam flow and cause solid particle erosion (SPE) in steam turbine components. The cracks leading to exfoliation most often do not traverse the full scale thickness. Hematite typically

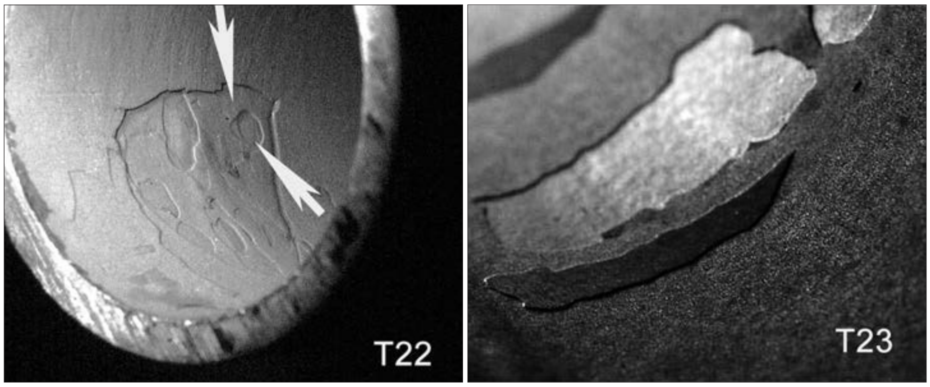

(a) (b)

Figure 14:
Examples of locations from which scale has exfoliated from T22 and T23, showing different behaviors.

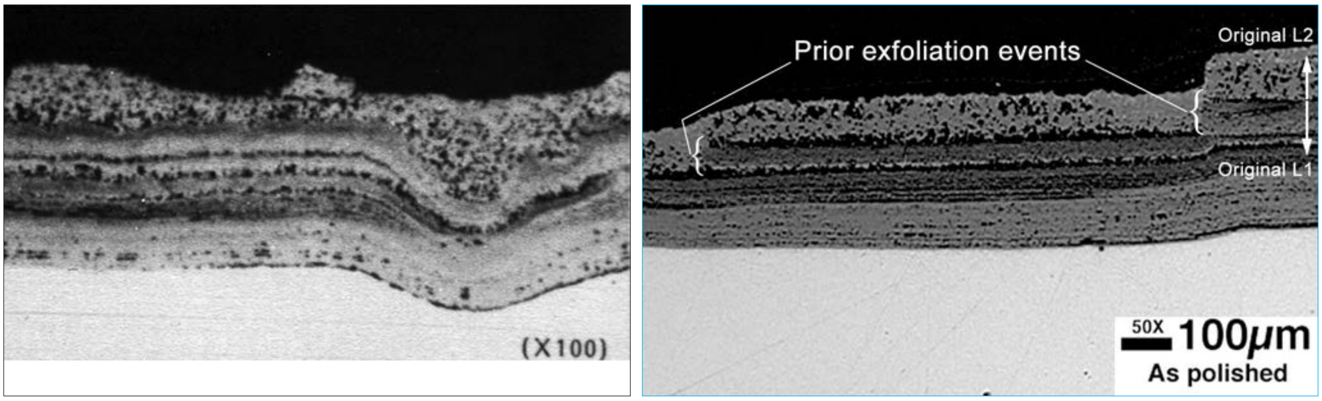

(a) (b)

Figure 15:
Examples of OGEI 5 for T22 showing thick multi-laminations and examples of locations from which exfoliation has occurred: (a) showing the morphology of the scale after a region has exfoliated, and (b) a nominally 360 µm-thick scale from which two prior exfoliation events have occurred (locations indicated by arrows).

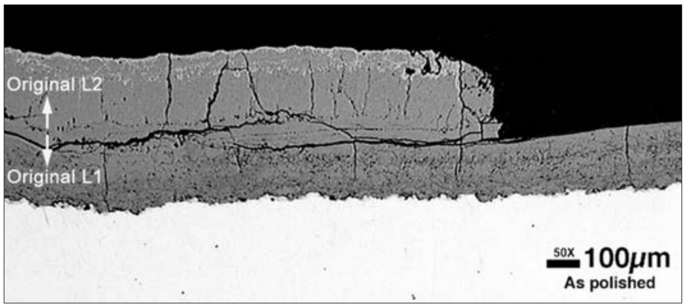

Figure 16:
An example of the typical exfoliation mode of T91, with separation of the full thickness of the original magnetite layer.

is present on these thick, laminated exfoliants (located on the steam interface of the original L1/magnetite of the initial duplex), but often is difficult to see because the flakes are very thick.

Exfoliation from T23 consists of much larger flakes than T11/22 (similar to those from austenitics), as shown in Figure 14b. This behavior is thought to relate to the varying thicknesses of the laminations in the main inner layer formed on T23.

For T91 the most common mode of exfoliation involves delamination of relatively long lengths of the outer magnetite layer with any associated hematite, as illustrated in Figure 16. The voids between and associated with the layers/bands in the original Fe-Cr spinel layer increase and coalesce to separate the Fe-Cr spinel from the original magnetite. These scale features are referred to as "delaminations," and start most frequently at the base of the original magnetite (Figure 17a). Occasionally, the delamination processes on T91 result in an exfoliant consisting of the original magnetite layer plus some fraction of the main inner layer. Sometimes there is oxide bridging associated with this delamination process to form closed "blisters," as shown in Figure 17b; such features have resulted in tube overheating and boiler tube failures (BTF).

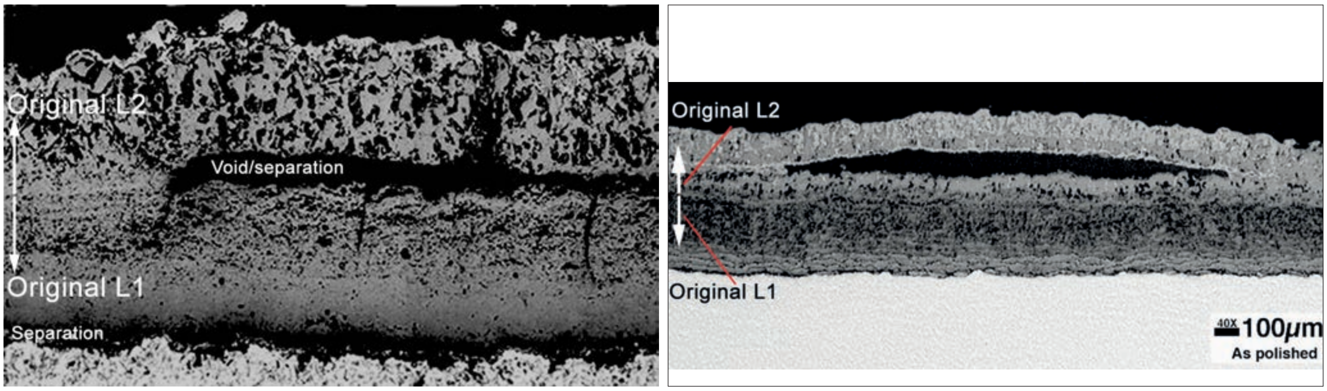

(a) (b)

Figure 17:
Example of OGEI 4 for T91, showing (a) distinct chromium rich bands in L1 and separation along the original L1-L2 interface on T91 after 61 000 h at temperatures up to 1 250 °F/670 °C, and (b) leading to the development of closed blisters (after 63 600 h at 1 051 °F/566 °C).

A further variation of exfoliation behavior observed with T91 is loss of the full scale thickness. The relatively few reported occurrences of this variant have involved service in heat recovery steam generators (HRSGs) that have experienced large thermal transients related to attemperation, condensate management, and inadequate drains [14]. The cause of this mode of scale loss has been attributed to the development of voidage along the metal-oxide interface, usually early in life.

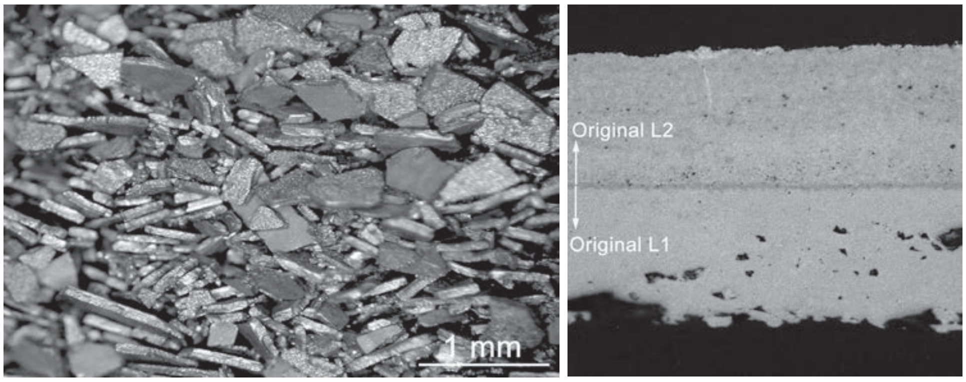

(a) (b)

Figure 18:
(a) Scale exfoliated from a P91 header of an HRSG, and (b) cross section showing full flake thickness. A small region of hematite is visible on the outside of the magnetite (L2) layer.

Figure 18a illustrates the mass of exfoliant collected from a P91 header in an HRSG, and the size and shape of individual flakes. These flakes clearly comprised the full thickness of the scale, Figure 18b.

### 2.2 Oxide Growth and Exfoliation Indices for Austenitic Steels – Alloys Considered: TP304H, 316H, 321H, 347H and HFG, 309, 310HCbN/ Alloy HR3C, and Internally-Treated Tubes (e.g., Shot-Peened) of TP304H

Unlike the ferritic steels considered, in which increasing alloy chromium content results in distinct changes in the morphology of the inner Fe-Cr spinel layer of the original duplex scale, for austenitic steels the major effect is an increase in the protectiveness of the Fe-Cr spinel without major morphological changes. While the level of chromium in the inner layer on austenitic steels initially is inherently higher than on these ferritic steels, with time the chromium level along the interface with the austenitic alloy can increase further, so that the inner layer becomes increasingly protective. This is because the Fe-Cr spinel has a variable crystal structure (typically described as $Fe_xCr_{2-x}O_4$) that can range from magnetite ($Fe_3O_4$) to chromite ($FeCr_2O_4$, with 46 wt% Cr). As a result, the overall inner layer on austenitic steels can have a chromium gradient while maintaining the same crystal structure/ morphology.

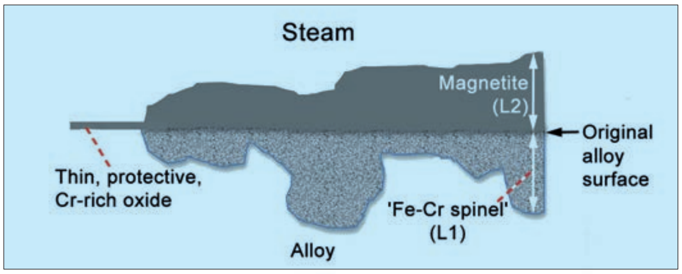

Figure 19:
Schematic diagram of a cross section of a typical initial scale formed in steam on "standard" austenitic steels.

A further outcome of this absence of significant morphological changes is that the scales formed in steam on austenitics maintain an essentially single duplex structure throughout their lives, which allows the layers to be unambiguously described as 'L1' and 'L2'.

### OGEI A: In this stage the characteristic duplex scale structure develops.

The morphology of the initial scales formed on "regular" austenitic steels can be very variable, depending on their actual levels of Cr, Ni, Mn, Si, Nb, and S, for instance, as well as differences in the surface condition of the tubes and the exposure conditions experienced during initial operation. Nevertheless, the scales rapidly assume the mostly duplex structure which typifies OGEI A, with a few areas where a very thin, protective (Cr-rich), single layer persists for some time, as suggested in Figure 19. The inner layer of the duplex structure is an Fe-Cr spinel (L1, magnetite containing Cr) and the outer layer is magnetite (L2), while the single-layered, thin scale typically is $FeCr_2O_4$, the highest-Cr version of the Fe-Cr spinel. At this point there are no voids at the L1-L2 interface, and no hematite in the outer part of

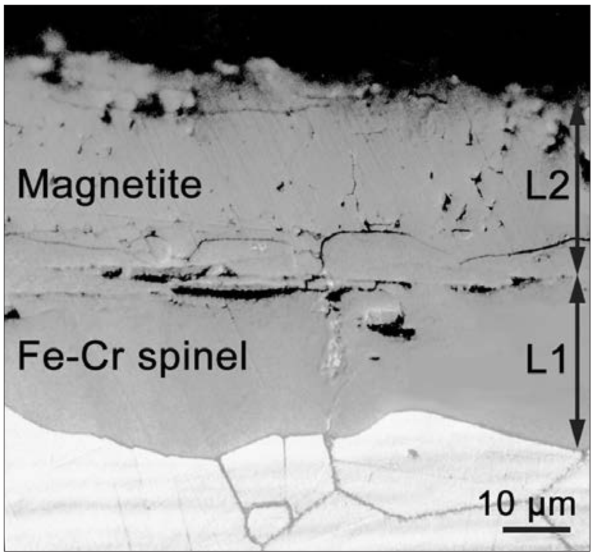

Figure 20:
Optical photomicrograph of metallographically-prepared cross section of scale formed on a "regular" austenitic (TP304H) showing an example of OGEI A.

L2; Figure 20 is an example of the OGEI A duplex scale structure on TP304H.

For alloys capable of forming a more protective initial scale, such as the higher-Cr austenitics TP309 and TP310HCbN/HR3C, as well as fine-grained austenitics (TP347HFG, Super304H), in stage OGEI A the bulk of the initial scale is much thinner, and first appears mostly as areas of thin, single-layered, Cr-rich oxide with isolated duplex islands (L1+L2); in some areas the L1-alloy interface is decorated with Cr-rich oxide which may encircle associated alloy grain boundaries (Figure 21). With time the areas of thin, single-layered oxide typically become converted to the double-layered structure, so that the overall scale morphology eventually resembles that on 'regular' austenitics, but remains notably thinner.

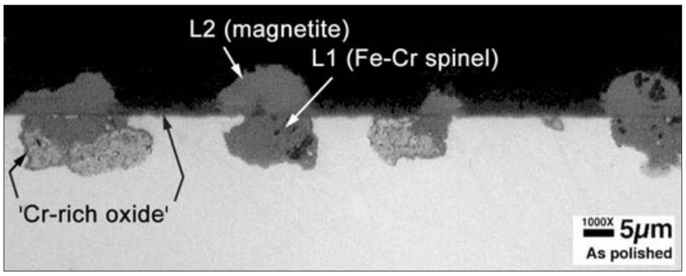

Figure 21:
Example of OGEI A on higher-Cr austenitic steels; the nodules have a duplex structure (L1+L2), and a thin layer of Cr-rich scale connects the nodules and partially encircles alloy grains near the surface.

Although the spinel structure of $FeCr_2O_4$ is energetically favored in austenitic steels, such that it forms more readily than the higher-Cr oxide chromia ($Cr_2O_3$, 68 wt%) [15], with time the oxide at the base of L1 on the higher-Cr and the fine-grained alloys can exceed the maximum of 46 wt% Cr corresponding to $FeCr_2O_4$, indicating that chromia also may be present. In such areas the basal scale would be expected to be more protective for longer times.

### OGEI B: This stage is characterized by the development of voids between the original duplex layers and the appearance of hematite in L2.

As the total oxide thickness increases and the ionic diffusion slows, voids begin to form at the L1-L2 interface, and gradually become more visible, Figures 22a and b. In addition, the amount of hematite in L2 increases until it occupies a large percentage of the cross section of that layer, though this feature can vary widely. These changes result from increasing blockage of movement of iron ions and oxidant in L1 due to the formation of increasingly Cr-rich oxide along the base of L1. Where such Cr-rich oxide completely occupies surface alloy grain boundaries, growth of L1 may be markedly slowed (or effectively stopped), with the result that the thickness of L1 becomes very uneven (as illustrated in Figure 22). Note that there is never (or almost never) any initiation and growth of laminations in L1 in the oxides formed on these austenitic steels.

### OGEI C: In this stage there develops an increasing density of voids along the L1-L2 interface and an increasing fraction of L2 is converted to hematite.

With increasing time and thickening of the total oxide the number of voids formed along the L1-L2 interface increases as blocking of transport through L1 continues to increase, and eventually a semi-continuous line of voids is developed, Figure 23. No breakdown of the structure of L1 is observed; instead this layer may become increasingly irregular in appearance due to continuing inward growth in some alloy grains, adjacent to regions where such growth has been effectively stopped by the formation of Cr-rich oxide along encircling alloy grain boundaries.

### OGEI D: In this stage separation occurs along the L1-L2 interface, and exfoliation of L2 begins.

The stresses between the oxides and austenitic steels that develop upon cooling are compressive and, further, since hematite has a signifi-

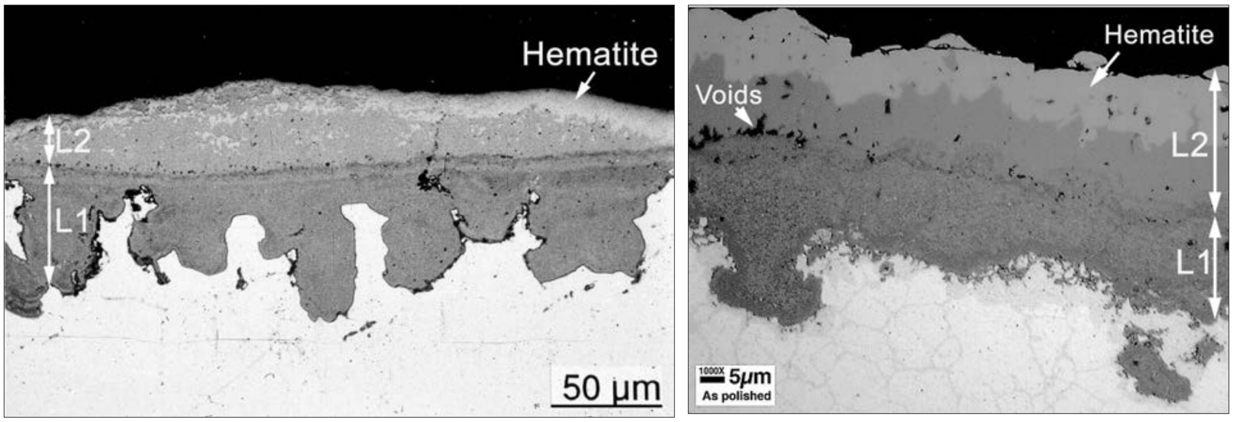

(a) (b)

Figure 22:
Examples of initiation of voidage along the L1-L2 interface on austenitic steels, and growth of hematite at the L2-steam interface: (a) TP304H, and (b) TP347H (4100 h at $T_s$ = 1085 °F/585 °C).

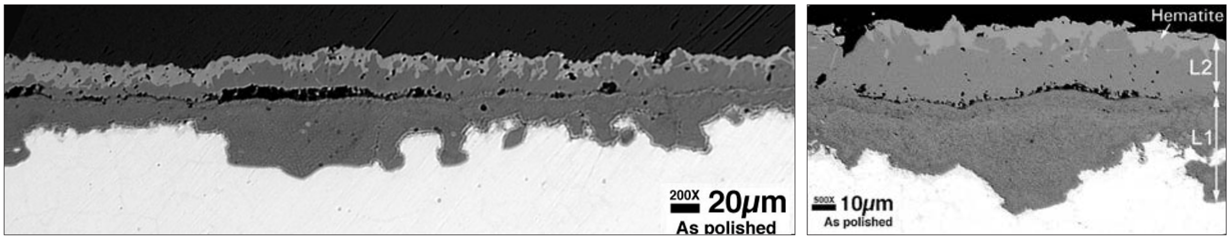

(a) (b)

Figure 23:
Examples of (a) development of voidage along the L1-L2 interface on "normal" austenitic steel, TP347H, and (b) growth of hematite at the L2-steam interface.

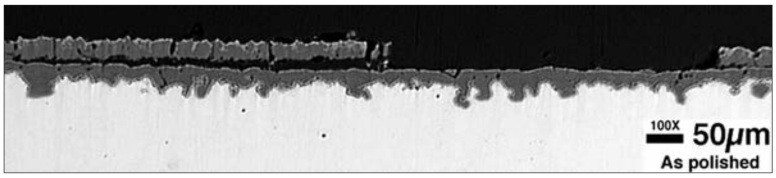

Figure 24:
Example of OGEI D for a "regular" austenitic, TP347H: separation has occurred along the L1-L2 interface and the whole thickness of L2 has been lost.

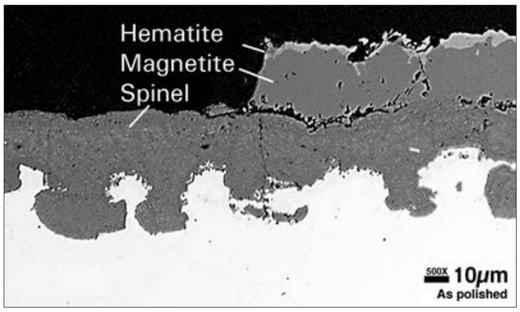

Figure 25:
Detail of exfoliation of the outer magnetite layer (L2) from TP347H, showing the clean separation between the Fe-Cr spinel (L1) and magnetite layers.

cantly lower CTE than the alloy and magnetite, its presence in L2 effectively increases the stress differential between L2 and the alloy/L1. With a sufficient temperature drop these compressive stresses are able to lead to scale exfoliation. It is important to realize that in normal boiler operation the maximum possible temperature drop, typically from service temperature to near ambient, is required to generate compressive stresses of the required magnitude. This implies that exfoliation events will not occur during shorter periods of shutdown (such as overnight, or at a weekend) when the tubes do not cool down fully.

Exfoliation from these austenitic steels results in detachment of the full thickness of L2 (including any hematite), as illustrated in Figures 24 and 25, and in some cases L2 is lost over long lengths of surface. However, loss of any part of L1 rarely occurs since L1 effectively is keyed to the alloy by the very irregular alloy-L1 interface. This results in the planes of weakness created by the areas of semi-continuous voidage along the L1-L2 interface becoming preferred paths along which stress relief can occur.

Typically, exfoliation initiates once the density of voids/cracks along the L1-L2 interface and hematite in L2 reaches a critical percentage. The authors suggest that this could involve typically more than 70 % of the interface between L1 and L2.

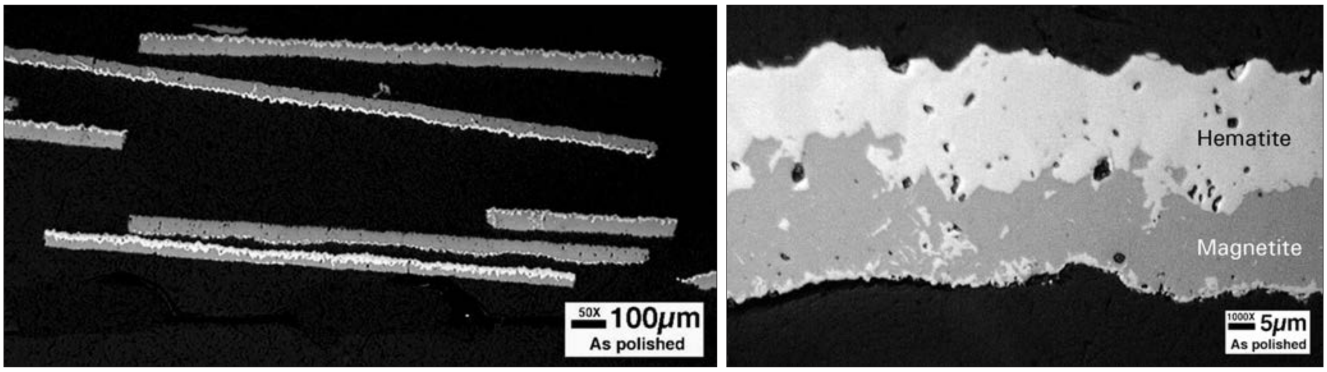

(a)

(b)

Figure 26:
Oxide flakes exfoliated from alloy TP347H after reheater service: (a) showing representative lengths of exfoliant, and (b) a cross section of a typical flake, showing it to consist of magnetite with a significant fraction of hematite.

Figure 26 illustrates metallographically-prepared cross sections of such exfoliated oxide flakes, which clearly consist of magnetite containing various fractions of hematite. In all cases there are indications of hematite along the prior L2-L1 interfaces.

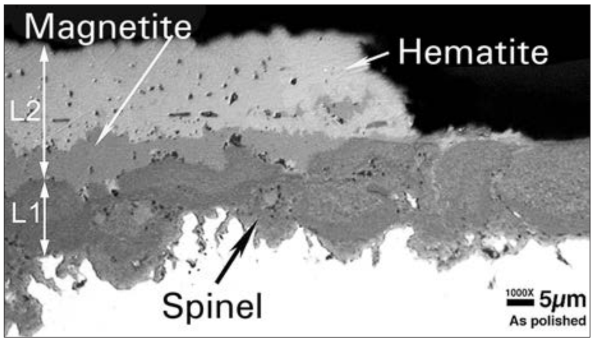

Figure 27:
Scale formed on fine-grained alloy TP347HFG after very high temperature service, showing exfoliation of a thin (22 µm) outer layer of scale consisting of 74 % hematite/26 % magnetite.

On fine-grained alloys where a high chromium content rapidly develops at the base of L1 and quickly shuts down outward transport of iron ions, L2 is more rapidly converted to hematite than on "regular" austenitics. Figure 27 shows a cross section of the scale formed on TP347H-FG after service at very high temperatures ($T_m$ > 1 200 °F/650 °C) on which hematite was at least 74 % of the thickness of L2. The maximum measured chromium content at the base of L1 was 59 wt% ($FeCr_2O_4$ is 46 wt%; $Cr_2O_3$ is 68 wt%), and exfoliation had occurred that involved the full thickness of L2 (hematite and remaining magnetite). The total scale thickness from which exfoliation had occurred was relatively small (approximately 35 µm), producing flakes of estimated thicknesses of 18–23 µm. These compare with an average thickness of flakes exfoliated from TP347H (Figure 26) of 48 µm for flakes with relatively thick layers of hematite, to 62 µm for flakes with very little hematite. The observation further supports the discussion that the presence of hematite increases the cooling stress differential, leading to exfoliation occurring from thinner scales.

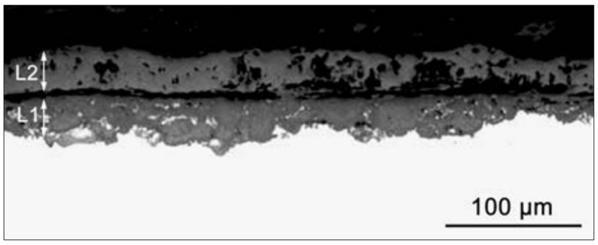

Figure 28:
Optical cross section of scale formed on shot-peened TP304H after RH service for 23 000 h at 1 112–1 157 °F/600–625 °C.

The adherent OGEI A-stage scale shown in cross section in Figure 28 was formed on shot-peened TP304H after service for 23 000 h at 600–625 °C in a final reheater. No exfoliation had occurred, even at a total scale thickness of 65 µm, whereas the scale formed on "normal" TP304H in the same unit had completely exfoliated in the same time. The elemental scanning electron microscope (SEM) X-ray images shown in Figure 29 suggest that the outer layer (L2) was quite adherent without obvious voids along the L1-L2 interface, so that the apparent interfacial crack evident in the optical image (Figure 28) was likely a result of metallographic preparation. There appears to be an essentially continuous Cr-rich oxide along the base of L1, which accounts for the protective nature of this scale.

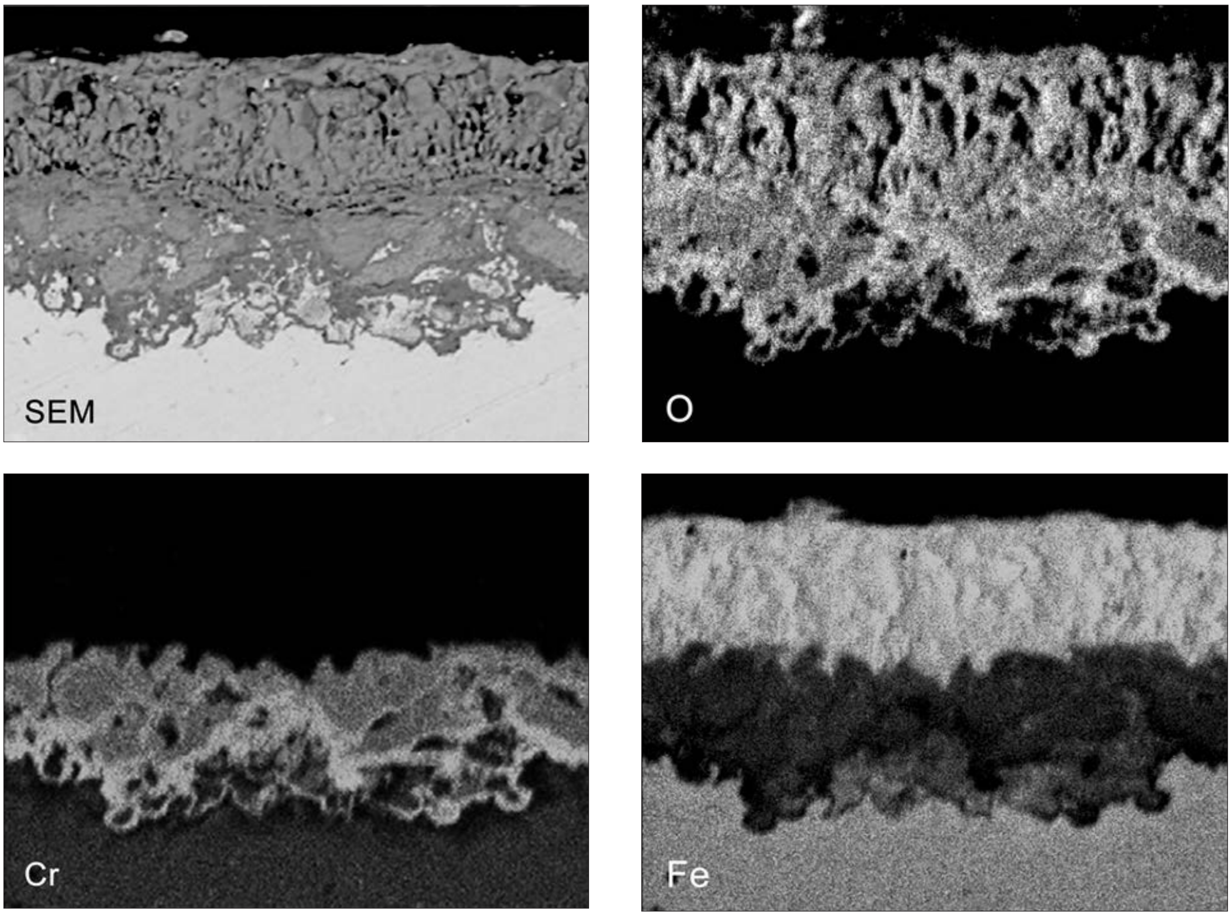

Figure 29:
SEM X-ray images for the scale shown in Figure 28.

### OGEI E: Following exfoliation of the outer magnetite layer (L2) there is some regrowth of oxide.

Figure 30 shows a cross section of the scale on a "regular" austenitic steel immediately following an exfoliation event in which the full thickness of the outer magnetite layer (L2) was lost. With subsequent exposure, growth of new oxide will occur on the newly-bare surface of L1, the rate of growth depending on the extent of completion of continuity of the layer of Cr-rich oxide at the base of L1. The new oxide (new L2) could be magnetite (as in OGEI A) or hematite, depending of the prevailing rate of transport of iron ions. In some cases, especially on fine-grained or shot-peened alloys, hematite forms almost 100% of the new growth. Figure 31 indicates the growth of hematite directly on the remaining original L1 on TP347HFG.

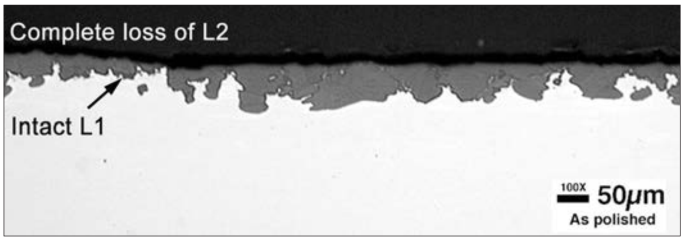

Figure 30:
Scale remaining on the surface of "regular" austenitic steel TP304H following an exfoliation event after 22000h at $T_s$ = 1005°F/538°C, in which all of the outer magnetite layer (L2) has exfoliated.

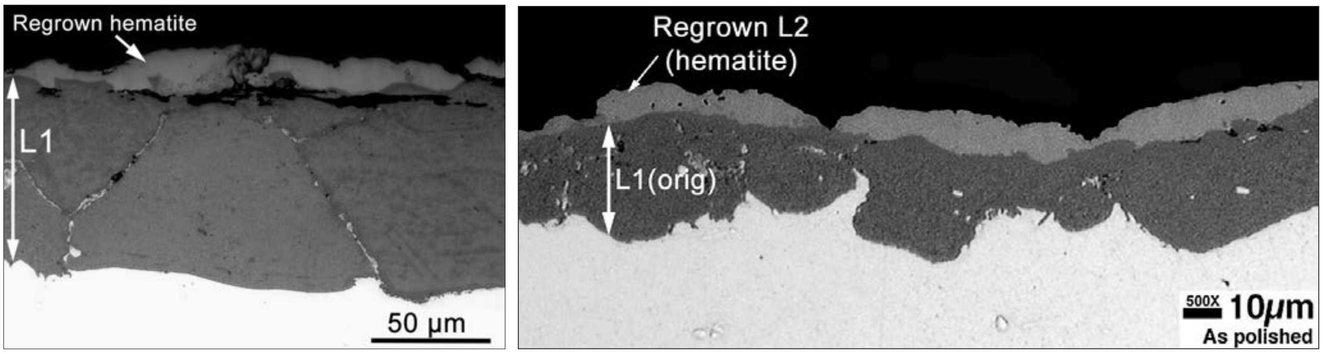

(a) (b)

Figure 31:
Illustrations of the regrowth of scale directly on the remaining inner layers (L1) on austenitic steels: (a) initial regrowth of hematite on L1, and (b) development of a continuous new outer layer consisting solely of hematite on fine-grained alloy TP347HFG.

## 3 APPLICATION OF OGEI TO GENERATING PLANT PROBLEMS

Section 2 has provided progressive morphologies of the oxides that grow on ferritic and austenitic steels in steam circuits of power generating plants. This progression goes from first operation with scales consisting of duplex pairs (Fe-Cr spinel and magnetite) to exfoliation on cool down due to differences in the coefficients of thermal expansion of the oxides and alloys. Both the growth and exfoliation processes can cause a wide range of reliability problems in these plants, sometimes in the superheater or reheater (RH), where the oxides actually grow, but also in other plant components in which exfoliated oxide flakes cause tube blockages. Because of differences in the morphologies and modes of exfoliation of the oxides grown on some of the alloys employed as SH and RH tubes, recognition of key features of recovered/collected exfoliant allows the source of the damaging particles to be identified. This approach can be used in root-cause investigations of the problems after the events but, probably more importantly, also to proactively identify future problems if samples of SH/RH tubing are removed for metallurgical analysis and identification of the OGEI.

Some of the well-understood problem areas can be identified as follows:

Figure 32:
Damage to first stage of an IP steam turbine due to SPE.

### 3.1 Solid Particle Erosion of Steam Turbine Components

This mechanism was researched extensively in the 1970s and 1980s and it is generally understood that the erosive particles are thick, multi-laminated oxide layers exfoliated from the low-Cr ferritic alloys (T11, T12, T22), such as illustrated in Figure 15. If they reach the turbine itself, damage can be severe, as illustrated in Figure 32.

### 3.2 Short-Term Overheating Boiler Tube Failures

This has been a worldwide BTF problem since the late 1960s (first cases involved austenitic steel TP316 in Scottish boilers). It has occurred predominantly in platen superheaters, but has also more recently occurred in a number of platen reheaters. The usual operating scenario is that the unit has operated continuously at high base load for long periods (sometimes up to a year or more) without shutting down to ambient. This allows the oxide morphology on austenitic alloys to progress to OGEI C as illustrated in Figure 23. Most often the unit then has a forced

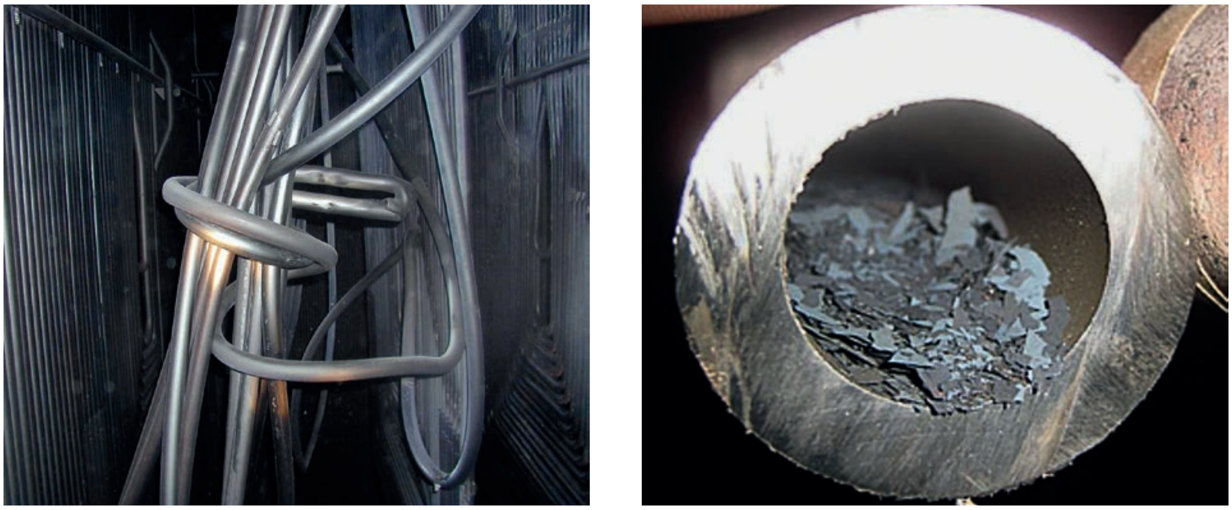

(a) (b)

Figure 33:
Massive deformation of tubes at the bottom of a platen superheater due to a STO failure (a) (courtesy of John Begg, Eskom, South Africa), from blocking by exfoliated oxide at a tube bend (b).

outage in equipment other than in a steam circuit, which requires the unit to be cooled to ambient. On return to service, just as the boiler is approaching full/high load, a BTF will occur in a SH/RH platen element. Sometimes the primary damage is immense, with grossly twisted tubes, as indicated in Figure 33a. The maintenance staff will repair the damage, and typically on return to service another BTF in another SH/RH platen will occur. This cycle has often been repeated 3 or 4 times, until it is recognized that these are shortterm overheating failures due to exfoliated oxide blocking the circuit at a bend at the bottom of the SH/RH platen; an example is shown in Figure 33b. The plant operator will then use various techniques to identify the blocked area, clear the blockage, and return the boiler to service. It is not unknown for further BTFs to occur.

The exfoliated oxide causing the blockage eventually will be identified as coming from the austenitic alloy tubing (as illustrated in Figures 24 and 25). There also are some observations that suggest that the oxide could originate from alloy T91 (such as illustrated in Figures 16–17). Here, using the described OGEI approach, the exact source of the exfoliated oxide can be determined by relating the metallography to OGEI 4 or OGEI D. It is also quite common to find in the debris causing the blockage examples of exfoliant from other SH/RH alloys located upstream of the failure location; again, using the OGEI, it is possible to identify the exact source. As expected from the discussion in Section 2.2, it is not surprising to note that the authors do not know of any STO BTF directly related to any exfoliation from shotpeened austenitic alloys.

### 3.3 Longterm Overheating

A very common BTF in SH/RH circuits is longterm overheating/creep (LTOC) due to excessive growth of steam-side oxide and accompanying loss of tube wall thickness. The tubing most often has a black and cracked appearance on the outside surface of the tubing (Figure 34).

Figure 34:
Typical appearance of a SH tube after failure due to LTO and creep.

For over 40 years boiler manufacturers have addressed the issue of excessive oxide growth by limiting tube temperatures to an Oxidation Limit (OL), which was previously referred to as the maximum temperature limit for tubing. These temperatures were derived from laboratory oxidation experiments and were well published for the low-chromium ferritic steels [2,16,17]. A most important criterion in boiler design is not to include tubing in a superheater or reheater that will exceed the OL for that tube material.

| Tube Material | Oxidation Limit | |
|---|---|---|
| | °F | °C |
| T12 | 1 022 | 550 |
| T11 | 1 049 | 565 |
| T22 | 1 076 | 580 |
| T23 | 1 103 | 595 |
| T91 | 1 120 | 605 |
| TP300-series austenitics (< 25 wt% Cr) | 1 292 | 700 |
| TP300-series austenitics (> 25 wt% Cr) | 1 382 | 750 |

Table 5:
Oxidation limits for superheater and reheater alloys.

Unfortunately, the same laboratory experiments have not been undertaken for newer ferritic steels (such as T23 and T91), and thus there has been a number of recent examples of the inclusion of these alloys in new boilers with design temperatures based only on maximum stress limits, which typically are higher than the OL. As a consequence, such tubes have experienced LTOC very early in life. Based on the authors' practical experience and from the OGE indices in Section 2.1, an updated list of OLs including these newer materials is suggested in Table 5. A recent publication has indicated a similar limit for T91 of 1 112 °F/600 °C [18].

It is well understood that as the oxide grows in thickness the resistance to heat transfer of the overall tube wall increases (rule of thumb is for every mil (25 µm) of oxide the temperature of the tube wall will increase by about 4 °F/2 °C). Proactive use of the OGEI can help to avoid this mechanism if tube samples are removed for metallurgical analysis, and the findings compared with the morphologies for the OGEI progressions.

OLs also have been established for austenitic steels used in steam boilers for almost 40 years [2,17,18], and a distinction was made between alloys containing less or more than 25 wt% Cr; the prevailing values are shown in Table 5. These values were derived from considerations of reduction of creep strength due to loss of tube wall section from the effects of environmental degradation, and typically are significantly lower than those associated with service in air [19,20]. Metal loss from corrosion on both the steam side and fireside was considered. In addition to any influence of reduced wall section on creep behavior, there is the further consideration that continuing increase in the thickness of corrosion scales will increase resistance to heat transfer through the tube wall, increasing tube temperature, and reducing lifetime. However, since in the experience of the authors instances of overheating (LTOC) of austenitics are rare, the relevance of these OLs for austenitic steels to boiler operation is not clear. They are listed here for completeness.

### 3.4 Erosion of Valves and Deposits in Steam Turbines

Deposits in steam turbines often influence generation and performance. Here collection and metallurgical examination of oxide samples from the areas of damage can lead to identification of an OGEI stage, which in turn can identify sections in the SH/RH where there might be an unknown overheating problem causing rapid steam oxidation and/or early exfoliation.

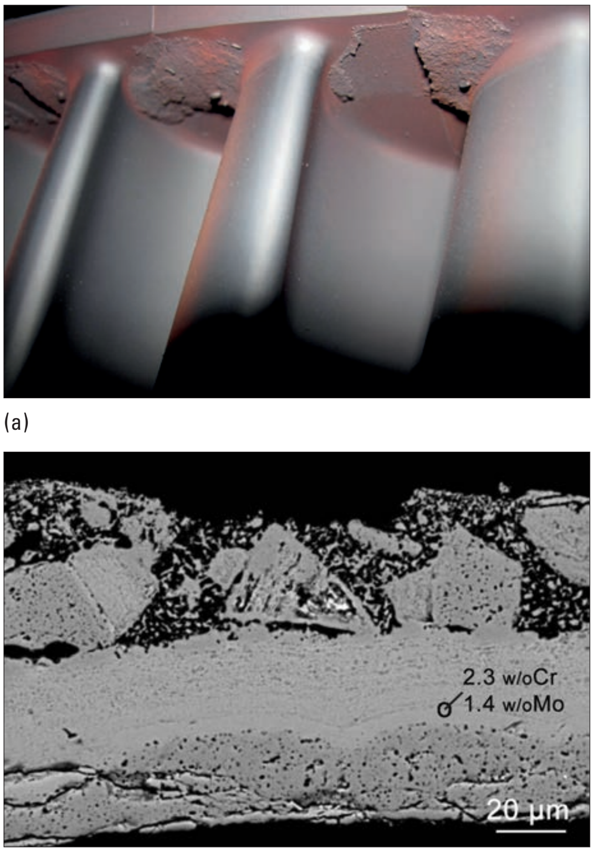

(a)

(b)
Figure 35:
Oxide deposits in a steam turbine: (a) typical appearance, and (b) deposit identified as stage OGEI 3 oxide from a T23 reheater.

Figure 35 shows an example of deposit in a steam turbine which was identified by metallurgical examination as originating from a stage OGEI 3 oxide formed on alloy T23 (as illustrated in Figure 8). Elemental mapping showed that the inner layer contained W and V (as in Figure 9). This further identified an emerging problem in the T23 section of the reheater, so that the local overheating could be addressed. In other cases, the depositing oxide may be from austenitic and/or ferritic steels, but in each case the OGEI can be identified and thus the location and material of concern.

### Deposits in Tubing and Other Places; Sticking Valves

The same process can be undertaken to identify exactly the source of the exfoliant. Also, in many cases the authors have used the OGEI process to show that sticking valves were not related to SH/RH exfoliation, but instead due to excessive levels of feedwater corrosion products (particulate and soluble).

### 3.5 Possible Increase of Total Iron Monitored in the Condensate

This is currently a very important item, such that the International Association for the Properties of Water and Steam (IAPWS) is developing new guidance for monitoring total iron on fast- and frequent-start units. The same process as described in the other examples can be used to identify the source of the total iron in the condensate.

## 4 SUMMARY, CONCLUSIONS, AND TOWARDS THE FUTURE

The paper describes two OGE indices: a) OGEI 1 to 5 for ferritic steels, and b) OGEI A to E for austenitic alloys. In each stage the progression of the oxide morphologies can be identified from the initial magnetite/Fe-Cr spinel duplex pair to those associated with exfoliation. In the case of ferritic steels exfoliation usually involves multiple layers of oxide, whereas for the austenitics exfoliation involves only the outer magnetite layer. Following the formation of the initial duplex growth on ferritic steels, the morphological development is clear and distinctly different on alloys T11/T12/T22 compared to T23 and T91, and the associated OGEIs can be used to define the exact stage in the progress to exfoliation. For austenitic alloys the morphological path to exfoliation is dependent on the formation of a chromium-rich oxide at the alloy/Fe-Cr spinel interface, and the OGEIs here allow distinction between austenitics that will exfoliate early or not at all. Examples have been included on the application of OGEIs to plant problems such as short- and longterm overheating tube failures, solid particle erosion of turbine blades, and various situations where deposition of exfoliant causes either damage or loss of plant performance.

## 5 ACKNOWLEDGMENTS

This has been a working lifetime activity of the authors, and we are grateful to the many people, organizations, and plants worldwide that have supported aspects of this work and provided superheater and reheater samples. Extensive thought and discussion on steam-grown oxides have been provided by: John Stringer, Steve Paterson, Peter Tortorelli, Michael Schütze, Adrian Sabau, Bruce Pint, and Tony Fry. Discussions with Jeff Henry on Oxidation Limits have also been useful. One of us (IGW) is grateful for continued support from the US Department of Energy, Office of Fossil Energy, and the Electric Power Research Institute while at the Oak Ridge National Laboratory (ORNL). Morphological characterization was conducted in association with Wendy Weiss (Structural Integrity Associates), and Hu Longmire, Larry Walker, and Dorothy Coffey of ORNL. Diane Dooley helped with the word processing and initial development of some of the tables.

## 6 REFERENCES

[1] Armitt, J., Holmes, D. R., Manning, M. I., Meadowcroft, D. B., Metcalfe, E., *The Spalling of Steam-Grown Oxide from Superheater and Reheater Tube Steels*, **1978**. Electric Power Research Institute, Palo Alto, CA, USA, EPRI Report No. FP-686.

[2] Dooley, R. B., McNaughton, W. P., *Boiler Tube Failures: Theory and Practice, Vol. 1: Boiler Tube Fundamentals*, **1996**. Electric Power Research Institute, Palo Alto, CA, USA, EPRI Technical Report No. 105261.

[3] Dooley, R. B., "Opening Remarks", *presented at the EPRI-NPL Workshop on Scale Growth and Exfoliation in Steam Plant*, **2003** (National Physical Laboratory, Teddington, England). Electric Power Research Institute, Palo Alto, CA, USA.

[4] Wright, I. G., Dooley, R. B., "A Review of the Oxidation Behavior of Structural Alloys in Steam", *International Materials Reviews* **2010**, 55(3), 129.

[5] Wright, I. G., Dooley, R. B., "Morphologies of Oxide Growth and Exfoliation in Superheater and Reheater Tubing of Steam Boilers", *Materials at High Temperatures* **2011**, 28(1), 40.

[6] Wright, I. G., Dooley, R. B., "Steam-Side Scale Morphologies Associated with Scale Exfoliation from Ferritic Steel T22", *Materials at High Temperatures* **2013**, 30(3), 168.

[7] *Technical Guidance Document: Volatile Treatments for the Steam-Water Circuits of Fossil and Combined-Cycle/HRSG Power Plants*, **2015**. International Association for the Properties of Water and Steam, IAPWS TGD3-10(2015). Available from http://www.iapws.org.

[8] Eberle, F., Kitterman, J. H., "Scale Formation on Superheater Alloys Exposed to High-Temperature Steam", *Behaviour of Superheater Alloys in High-Temperature-High-Pressure Steam (Ed.: G. E. Lien)*, **1968**. American Society of Mechanical Engineers, New York, NY, USA, 67.

[9] Holcomb, G. R., "A Review of the Thermal Expansion of Magnetite", *Materials at High Temperatures* **2019**, 36(3), 232.

[10] Dooley, R. B., Paterson, S. J., Wright, I. G., "Oxide Growth and Exfoliation in Steam – Plant Experience", *presented at the EPRI-NPL Workshop on Scale Growth and Exfoliation in Steam Plant*, **2003** (National Physical Laboratory, Teddington, England). Electric Power Research Institute, Palo Alto, CA, USA.

[11] Schütze, M., *Protective Oxide Scales and Their Breakdown*, **1997**. John Wiley & Sons Ltd, Chichester, United Kingdom.

[12] Evans, H. E., Lobb, R. C., "Conditions for the Initiation of Oxide Scale Cracking and Spallation", *Corrosion Science* **1984**, 24(3), 202.

[13] *Atlas of Oxide Scales Formed on Superheater and Reheater Tubes*, **2015**. Electric Power Research Institute, Palo Alto, CA, USA, EPRI Report No. 3002006598.

[14] Dooley, R. B., Anderson, R. A., "Trends in HRSG Reliability – A 10-Year Review", *PowerPlant Chemistry* **2019**, 21(3), 158.

[15] Hansson, A. N., Pantleon, K., Grumsen, F. B., Somers, M. A. J., "Microstructure Evolution during Steam Oxidation of a Nb Stabilized Austenitic Stainless Steel", *Oxidation of Metals* **2010**, 73(1–2), 289.

[16] *Combustion, Fossil Power Systems: A Reference Book on Fuel Burning and Steam Generation (Ed.: J. G. Singer)*, **1981**. Combustion Engineering, Inc., Windsor, CT, USA, 3rd Edition.

[17] Kitto, J. B., Stultz, S. C. (Eds.), *Steam: Its Generation and Use*, **2005**. The Babcock & Wilcox Company, Barberton, OH, USA.

[18] *Grade 91 Use-Temperature Limits*, **2017**. Electric Power Research Institute, Palo Alto, CA, USA, EPRI Report No. 3002011137.

[19] Morris, L. A., "Generally-Accepted Maximum Service Temperature in Air for AISI Stainless Steels", *Handbook of Stainless Steels (Eds.: D. Peckner, I. M. Bernstein)*, **1977**. McGraw-Hill, New York, NY, USA, Chapter 17-1.

[20] *High-Temperature Characteristics of Stainless Steels*, **1979**. Produced by the American Iron and Steel Institute, Washington, D.C., USA and distributed by the Nickel Development Institute, A Designer's Handbook Series No. 9004.

## AUTHORS

**Barry Dooley** (B.Eng. with first class honours in Metallurgy and Ph.D. in Oxidation of Metals, both from University of Liverpool, UK; D.Sc. in Power Plant Chemistry from the Moscow Power Institute (University), Moscow, Russia) is a Senior Associate with Structural Integrity Associates (SI) in the UK. Before joining SI he was a Technical Executive, Materials and Chemistry, at the Electric Power Research Institute (EPRI) in Palo Alto, California, and Charlotte, North Carolina, specializing in Cycle Chemistry, Boilers, HRSGs, Steam Turbines, and Materials, as well as managing the Boiler and HRSG Tube Failure Reduction/Cycle Chemistry Improvement and FAC Programs. Before joining EPRI, he provided Cycle Chemistry and Materials Services for the fossil fleet at Ontario Hydro in Toronto, Canada, and conducted oxidation research in the Materials Division of the Central Electricity Research Laboratories (CERL) of the former Central Electricity Generating Board (CEGB) at Leatherhead, Surrey, England. Dr. Dooley is the author or co-author of over 290 papers in the areas of metallurgy, power generation, boiler and HRSG tube failures, FAC, cycle chemistry, steam turbine failures, and life extension and assessment of fossil plants. He is the Executive Secretary for the International Association for the Properties of Water and Steam (IAPWS), where he is an Honorary Fellow and chairs the development of the IAPWS Technical Guidance Documents for the cycle chemistry of power plants. Dr. Dooley organizes and chairs boiler/HRSG and chemistry forums and users group meetings worldwide.

**Ian G. Wright** (B.Sc. Tech., Chemical Engineering, M.Sc. and Ph.D., Corrosion Science from the University of Manchester) worked at Battelle-Columbus (1971–1994) and the Oak Ridge National Laboratory (1995–2010) before establishing WrightHT, Inc. In 1993–94 he was a Visiting Scientist at EPRI, Palo Alto. His career has focused on the application of mechanistic understanding of materials behavior to address the causes of shortcomings, as well as the issues confronted when applying materials near the limits of their capabilities. Promotion of these activities has involved serving on materials panels for major United States Department of Energy (DOE) and EPRI-funded projects, as well as peer review panels for corrosion research at NASA and various universities. He also has co-organized and co-chaired several major conferences. At Battelle-Columbus he was involved in alloy development and qualification projects, while among his activities at ORNL was management of materials aspects of DOE's Advanced Turbines Systems program and the Ultra-Supercritical Steam Materials program. In addition, he was Director of the Laboratory's Fossil Energy Program, and co-founded the UK-US Collaboration on Energy Research. He has authored/co-authored over 200 peer-reviewed papers, as well as over 100 others, and has made over 150 presentations at major meetings. He is a Fellow of NACE and ASM International.